

1 Generation of autogenic knickpoints in laboratory landscape
2 experiments evolving under constant forcing.

3

4 Léopold de Lavaissière¹, Stéphane Bonnet¹, Anne Guyez¹, and Philippe Davy²

5 ¹ GET, Université de Toulouse, CNRS, IRD, UPS(Toulouse), France,

6 ² Univ Rennes, CNRS, Géosciences Rennes - UMR 6118, 35000 Rennes, France,

7 Correspondence to: Stéphane Bonnet (stephane.bonnet@get.omp.eu)

8

9 ABSTRACT

10 The upstream propagation of knickpoints in river longitudinal profiles is commonly assumed to
11 be related to discrete changes in tectonics, climate or base-level. However, the recognition that
12 some knickpoints may form autogenically, independent of any external perturbation, may
13 challenge these assumptions. We investigate here the genesis and dynamics of such autogenic
14 knickpoints in laboratory experiments at the drainage basin scale, where landscapes evolved in
15 response to constant rates of base-level fall and precipitation. Despite these constant forcings, we
16 observe that knickpoints regularly initiate in rivers at the catchments' outlet throughout the
17 duration of experiments. The upstream knickpoint propagation rate does not decrease
18 monotonically in relationship with the decrease of drainage area, as predicted by stream-power
19 based models, instead the propagation rate first increases until the mid-part of catchments before
20 decreasing. To investigate the dynamics of the knickpoints, we calculated hydraulic information
21 (water depth, river width, discharge and shear stress) using a hydrodynamic model. We show that
22 knickpoint initiation at the outlet coincides with a fairly abrupt river narrowing entailing an
23 increase in their shear stress. Then, once knickpoints have propagated upward, rivers widen
24 causing a decrease in shear stress and incision rate, and making the river incision less than the
25 base-level fall rate. This creates an unstable situation which drives the formation of a new

Supprimé: upward

Supprimé: of rivers

Supprimé: independently

Supprimé: interpretations

Supprimé: landscape

Supprimé: duration

Supprimé: of knickpoint

Supprimé: their

Supprimé: but it

Supprimé: their

Supprimé: entailing

Supprimé: lower thanthe

38 knickpoint. The experiments suggest a new **autocyclic** model of **knickpoint** generation controlled
39 by river width dynamics **independent** of variations **in** climate or **tectonics**. This questions an
40 interpretation of landscape records focusing only on climate and tectonic changes without
41 considering autogenic processes.

Supprimé: cyclic and autogenic

Supprimé: knickpoints

Supprimé: regardless

Supprimé: any

Supprimé: of

Supprimé: tectonic rates

42 1 Introduction

43 Knickpoints are discrete zones of steepened bed gradient that are commonly observed in river
44 longitudinal profiles. Although they occasionally occur due to changes in bedrock properties (e.g. Duvall
45 et al., 2004), in many cases they are **dynamic** features that propagate upstream along drainage networks
46 (Whipple and Tucker, 1999; Kirby and Whipple, 2012; Whittaker and Boulton, 2012). In this **latter** case,
47 they are commonly considered as formed in response to variations in external forcing such as uplift rate,
48 sea level or climate (e.g. Crosby and Whipple 2006; Berlin and Anderson, 2007; Kirby and Whipple,
49 2012; Whittaker and Boulton, 2012; Mitchell and Yanites, 2019) which opens the possibility of using
50 knickpoints in landscapes to identify such changes. Several studies pointed out, however, that some
51 knickpoints could be autogenic, that is to say internally-generated without any variation in boundary
52 conditions (e.g. Hasbargen and Paola, 2000, 2003; Finnegan and Dietrich, 2011). Understanding how
53 knickpoints can form autogenically is therefore crucial for **interpreting** changes in external forcing from
54 **knickpoint** occurrence in landscapes. Most observations of autogenic knickpoints formation come from
55 experimental modelling (see for example Paola et al., 2009) their initiation being attributed to
56 amplification of local instabilities in flume (Scheingross et al., 2019) and drainage basin scale
57 (Hasbargen and Paola, 2000), experiments. In these latter experiments for example, successive
58 knickpoints initiated despite constant external forcing (base-level fall and precipitation) throughout the
59 duration of the runs, even when landscapes were at steady-state on average in terms of sediment flux.
60 Internal processes may also complexify the propagation of knickpoints as shown in the flume
61 experiments of Cantelli and Muto (2014) and Grimaud et al. (2016) where a single discrete event of
62 base-level drop **resulted** in the propagation of multiple waves of knickpoints.

Supprimé: dynamical

Supprimé: last

Supprimé: retrieving

Supprimé: their

Supprimé:)

Supprimé: result

63 .

76 In this work, we consider the generation and dynamics of autogenic knickpoints in laboratory-scale
77 drainage basins experiments forced by constant rate of base-level fall and steady precipitation. Such
78 landscape experiments have been used successfully to explore how tectonics and climate impact erosion
79 processes and the evolution of topography under controlled conditions (e.g. Hasbargen and Paola, 2000;
80 Bonnet and Crave, 2003; Lague et al., 2003; Turowski et al., 2006; Bonnet, 2009; Singh et al., 2015;
81 Sweeney et al., 2015; Moussirou and Bonnet, 2018). This approach allows for the observation of
82 complex dynamics that are sometimes difficult to simulate numerically and sheds new light on the way
83 natural landforms may evolve. Landscape experiments capture the tree-like structure of drainage
84 networks, the supply of eroded material from hillslopes, and especially their fluctuations, which is a
85 natural complexity that is not reproduced in flume experiments, for example. The experiments presented
86 here have been performed using a new setup specifically designed to investigate the evolution of a large,
87 meter-long, single drainage basin under controlled forcing condition. In previous similar catchment-
88 scale experiments (Hasbargen and Paola, 2000, 2003; Bigi et al., 2006; Rohais et al., 2012) the outlet
89 location was pinned to a narrow motor-controlled gate used to simulate base-level fall and which also
90 set the river width at the outlet. A specificity of our setup here is to use a large gate instead of a narrow
91 one, allowing experimental rivers to freely evolve downstream, with no constraints on their width. We
92 report here results from experiments where successive knickpoints initiate near the outlet autogenically
93 and propagate within drainage basins. The experiments show a new model of autogenic knickpoint
94 initiation and propagation driven by downstream river width dynamics.

Supprimé: d

Supprimé: emphasize

Supprimé: ¶

95 96 **2 Methods**

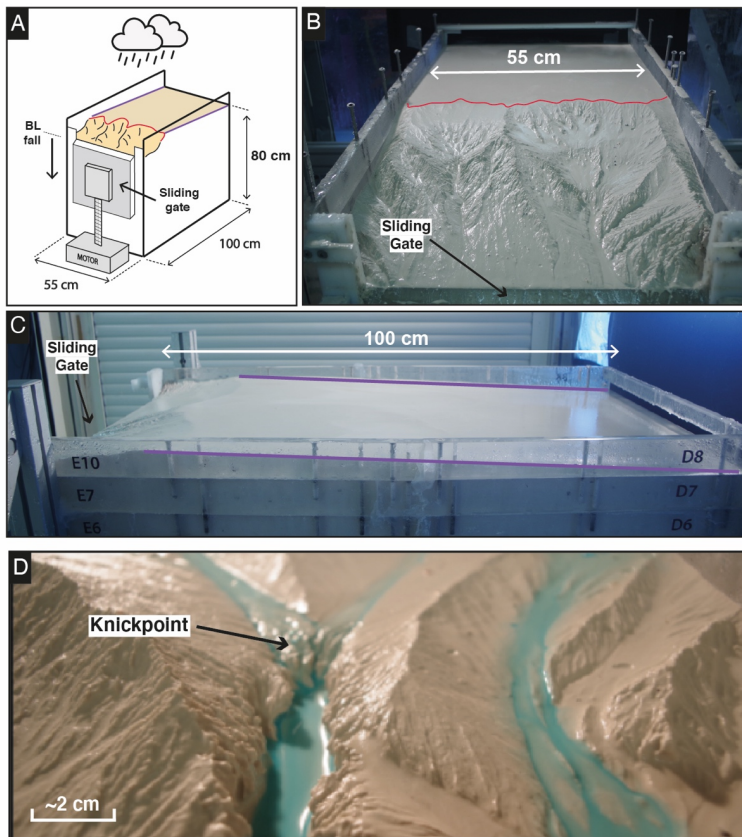
97 We present here results from 3 experiments, BL05, BL10 and BL15, performed with different rates of
98 base level fall, of respectively 5, 10 and 15 mm.h⁻¹ (Table 1). The facility is a box with dimensions 100
99 x 55 cm filled with silica paste (Fig. 1; see also Fig. S1 in the Supplemental Material). At its front side,
100 a sliding gate, 41 cm-wide, drops down at constant rate, acting as the base level. The initial surface
101 consists on a plane with a counterslope of ~3°, opposite to the base level-side (Fig. 1C). During a run,
102 runoff-induced erosion occurs in response to steady base level fall and rainfall (mean rainfall rate is 95

Supprimé: .

Supprimé: of

109 mm.h⁻¹ with a spatial coefficient of variation (standard deviation/mean) of 35%. Incision initiates at
 110 some point along the base level and propagates upstream until complete dissection of the initial surface.
 111 Note that the counterslope of the initial surface allows separating the rainfall flux between the base level
 112 and the opposite side of the device, creating a water divide (Fig. 1B).

Supprimé: .
 Supprimé: %). The mean spatial precipitation rate of each experiment is of 95 mm.h⁻¹. Incisions initiate
 Supprimé: propagate
 Supprimé: a
 Supprimé: surface allows to separate
 Supprimé: and then to create



113
 114 **Figure 1.** Experimental setup. Purple and red lines show respectively the counter-slope of the initial
 115 topography and the main water divide. (A) Sketch of the erosion box with the sliding gate, 41 cm wide,
 116 used to drop down the base level (BL). (B), (C) Front and side photographs (experiments BL10 at [525](#)
 117 [min](#) and BL15 at [185 min](#)). (D) Photograph of a typical knickpoint studied here.

Supprimé: 525'
 Supprimé: 185'

128 *Table 1. Parameters of experiments*

Experiments	Base Level Fall (mm/h)	Precipitation Rate (mm/h)	Duration Time (min)	Mean Divide Retreat Rate (mm/h)	nDDVmax*	Mean Knickpoint Retreat Rate (mm/h)
BL15	15	95	1065	66.3	0.52	183.6 ± 93.8
BL10	10	95	1200	55.7	0.57	164.8 ± 74.8
BL05	5	95	1455	25	0.54	73.1 ± 50

*nDDVmax : normalized distance of maximum knickpoint velocity

129 Experiments were stopped every 5 min to digitize the topography using a laser sheet and to construct
 130 Digital Elevation Models (DEMs) with a pixel size of 1 [mm²](#). Longitudinal profiles and knickpoints
 131 were extracted with a semi-automatic procedure that had to be developed to process the ~200 DEMs per
 132 experiment. For this purpose, we first extracted longitudinal profiles by [finding](#) the lowest elevation on
 133 successive rows ([lines oriented parallel to the sliding gate](#)) of each DEM within a 20 cm-wide swath
 134 [perpendicular to the sliding gate](#) that included the main river ([the one with the largest catchment for each](#)
 135 [experiment](#)). [Then the lowest elevation found in our search was plotted](#) against distance down the long
 136 axis of the box. This procedure has already been applied by Baynes et al. (2018) and Tofelde et al.
 137 (2019). It may result in a slight overestimation in channel slope because it does not consider the obliquity
 138 of channels within the box in the distance calculation nor their sinuosity. However, these effects are of
 139 minor influence here, because most channels are straight and roughly parallel to the long side of the box.
 140 In a second step, we computed the [erosion rates by considering](#) elevation difference between each
 141 successive pairs of longitudinal profiles and we identified knickpoints as peaks in erosion rates with
 142 values above the steady erosion amount defined by the rate of base-level fall (Fig. 2). We verified
 143 manually that this procedure defines knickpoints correctly by checking the computed positions on
 144 longitudinal profiles. We investigated in particular if the procedure is robust with respect to the time
 145 interval between successive profiles. We found that the record interval of 5 minutes is too small to
 146 produce well-defined erosional peaks, which lead us to identify knickpoint positions from a time-interval
 147 of 10 minutes. Then, we built a first catalogue of knickpoints positions at different times [from which we](#)
 148 manually extract the successive positions of each individual knickpoint. We complemented the database
 149 by computing incremental retreat rates of knickpoints from their successive positions.
 150

Supprimé: mm

Supprimé: considering

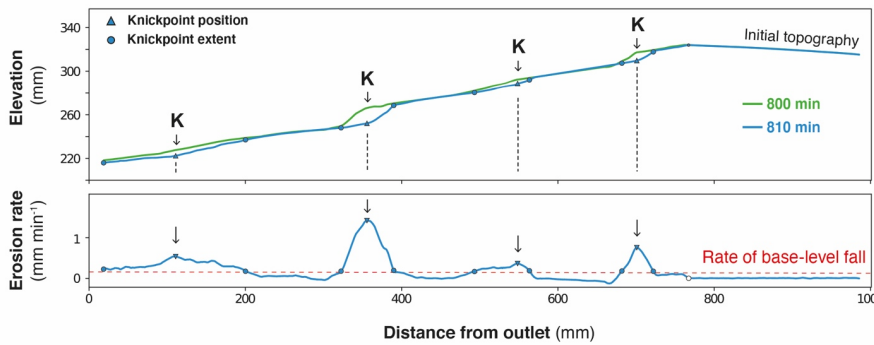
Supprimé: the

Supprimé: and then by plotting it

Supprimé: of

Supprimé:

151



158

159 **Figure 2.** Graph showing two successive longitudinal profiles of experiment BL10 taken at 10 min
 160 interval (top) and corresponding erosion rate profile (bottom). Triangles illustrate the position of
 161 erosional peaks taken as knickpoint position (black arrows). Red dashed line shows the rate of base-
 162 level fall.

163

164 DEMs were also used to compute hydraulic information (water depth, river width, discharge and shear
 165 stress) using the Floodos hydrodynamic model of Davy et al. (2017; see also Baynes et al. (2018,
 166 2020) for previous use of Floodos for analyzing laboratory experiments). Floodos is a precipitation-based
 167 model that calculates the 2D shallow water equations (SWE) without inertia terms, from the routing of
 168 elementary water volumes on top of topography. We ran Floodos on successive DEMs of experiments
 169 by [inputting](#) spatial distribution of precipitation, then generating several output raster products at the
 170 pixel size, including water depth, unit discharge and bed shear stress that were then used for
 171 computation of hydrologic parameters (river width, specific discharge and shear stress). The solution
 172 of the SWE depends on the friction coefficient (C) that depends on water viscosity only for laminar
 173 flow; its theoretical value is $\sim 2.5 \times 10^6 \text{ m}^{-1} \text{ s}^{-1}$ at 10°C (Baynes et al., 2018). To ensure that Floodos
 174 outputs (e.g. water depth raster maps) calculated using this value are consistent with actual experiment
 175 hydraulic conditions, we injected dye in the rainfall water during a run to catch the actual extent of
 176 water flow and make rivers visible. A visual comparison with Floodos results shows a good match
 177 between model outputs and experimental results (Fig. S2), which validates the numerical method and

Supprimé: considering

Supprimé: .

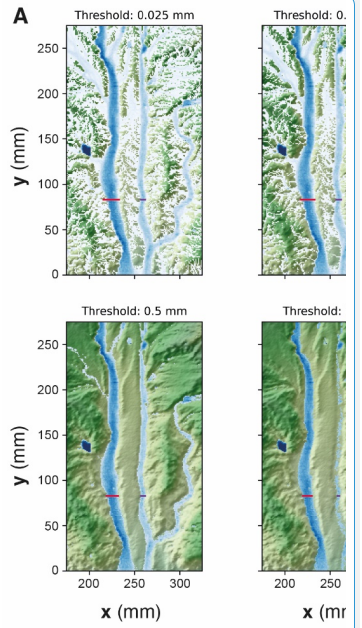
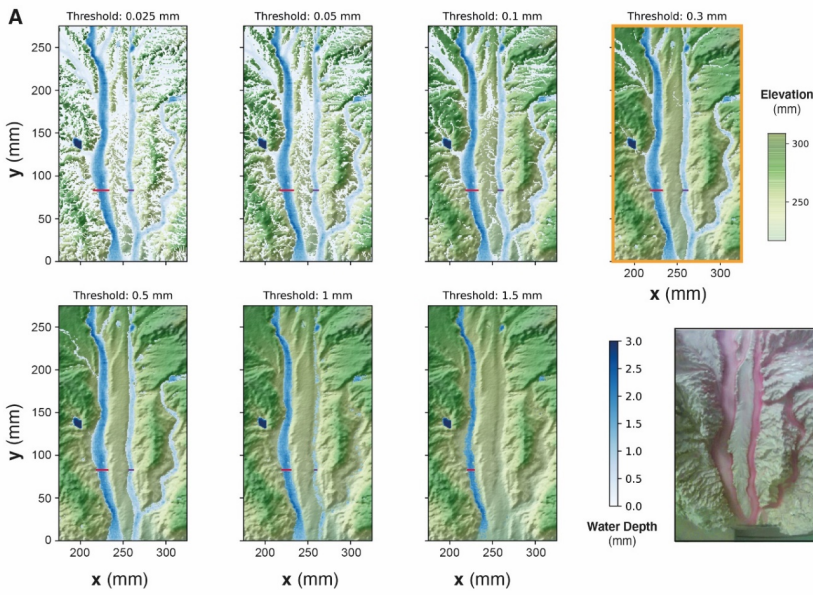
180 the expected theoretical friction coefficient C (Baynes et al., 2018). Given the difficulty to measure the
 181 mm-scale water depth without perturbating the flow, river widths were extracted from Floodos DEM
 182 outputs by thresholding the water depth maps considering that river banks correspond to sharp
 183 variations in water depth. The water depth threshold was estimated by trial and error by comparing the
 184 the rivers extracted from the calculation with direct observations on experiments where rainwater was
 185 colored by red dye (Fig. 3). A good visual agreement was obtained for a threshold value of the water
 186 depth between 0.1 and 0.5 mm, and a mid-value of 0.3 mm was then used for determining river
 187 widths.

Supprimé: perturbating

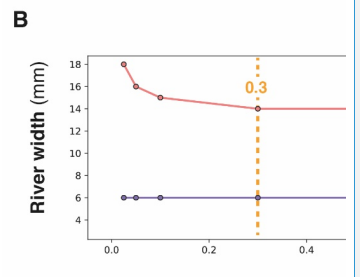
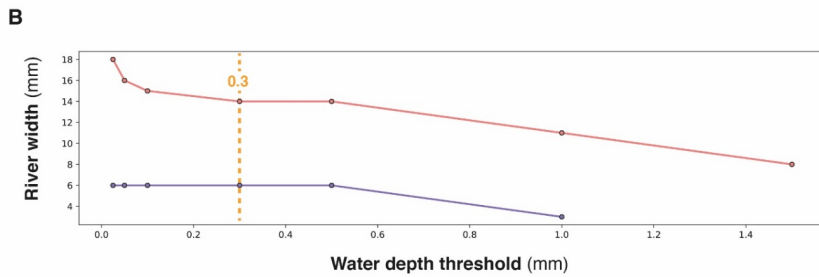
Supprimé: ,

Supprimé: corresponding

188



Supprimé:



189

194 **Figure 3.** Impact of water depth threshold used to delineate river boundaries on estimated river widths,
 195 A. Map views of water depths (blue colors) superimposed to DEM, for water depth threshold values
 196 between 0.025 and 1.5 mm. Red and purple lines show corresponding river widths for two rivers. Photo
 197 on the bottom right shows the active river width during the corresponding experimental run (“control
 198 run”), viewed by injecting red dye in the water used to generate the artificial rainfall. B. Corresponding
 199 local river widths for the two sections shown by red and purple lines. A threshold value of between 0.1
 200 and 0.5 mm shows a good similarity between rivers on water depth map and the control run. Here, a
 201 mid-value of 0.3 mm has been chosen for computing river widths.

Supprimé: , considering a friction coefficient C of 2.5×10^6
 $m^{-1} s^{-1}$

Supprimé: s

Supprimé: The use of a low water depth threshold value (e.g. 0.025 mm; top left) leads to the inclusion of large areas of shallow water depth in the “wetter area” considered as rivers and then to unrealistic large rivers in comparison with actual rivers observed in the control run. On the opposite, considering large threshold value (e.g. 1.5 mm) results in narrow rivers, or even in the absence of rivers when maximum computed water depth is lower than this threshold.

203 3 Results

204 3.1 Dynamics of knickpoints retreat

205 In each experiment, base level fall induces the growth of drainage networks by headward erosion and
 206 the progressive migration of a main water divide (Fig. 4). The migration rate of the divide is constant in
 207 each experiment (Fig. 5 and Table 1), and this value increases from 25 to 66 $mm \cdot h^{-1}$ with prescribed rate
 208 of base level fall of 5 to 15 $mm \cdot h^{-1}$. The successive longitudinal profiles of the main river investigated
 209 in each experiment (Fig. 6) illustrate the growth of rivers as they propagate within the box. These profiles
 210 show alternations of segments with low and high slopes, the latter defining knickpoints. Knickpoints
 211 regularly initiate at the outlet throughout the duration of the runs in all experiments and propagate
 212 upward until they reach and merge with the divide, some profiles showing even several knickpoints that
 213 retreat simultaneously (Fig. 6). A characteristic of these knickpoints highlighted in Figure 7 (see also
 214 Fig. 6) is that they generally initiate downstream with a gentle slope and gradually steepen as they
 215 migrate upstream. Their maximum slope is generally reached when they have propagated to the central
 216 part of the profiles (see below). Then the slope is maintained or slightly decreases during their retreat in
 217 the upper segment of the profiles.

Supprimé: .

Supprimé: of base

Supprimé: higher

Supprimé: They

218 The mean retreat velocity of knickpoints varies between experiments from 73 ± 50 to 183 ± 94 $mm \cdot h^{-1}$
 219 (Table 1) and increases as a function of the rate of base-level fall. Data suggest a non-linear relationship

Supprimé: ¶

Supprimé: .

237 between base-level fall rate and mean retreat velocity of knickpoints, however complementary
238 experiments would be necessary to constraint this dependency. To investigate the propagation of the
239 knickpoints, we built space-time diagrams (Fig. 8) by [plotting](#) the successive alongstream position of
240 each knickpoint over experimental runtime, as well as the position of the water divide in the box as
241 already reported in Figure 5. To compare the dynamics of knickpoints within an experiment regardless
242 of the stage of water divide retreat into the box, the position of knickpoints (distance to outlet, D) has
243 been normalized to the position of the divide, hereafter referred to as normalized distance to divide
244 (nDD; $nDD=0$ at outlet and $nDD=1$ at the divide; [Fig. 4](#)). Lines of isovalue of nDD considering an
245 increment of 0.1 are also shown in the space-time diagrams (Fig. 8). To a first order, the trajectories of
246 each knickpoint are very comparable within an experiment regardless the stage of retreat of the water
247 divide and the size of the catchment. Visually for example, in the space-time diagrams there is no
248 systematic variation in the general slope of the successive knickpoint trajectories over time, as the rivers
249 expand, that would indicate a change in mean knickpoint velocity in relation to the change in the river
250 length and catchment size. In detail, an inflection of trajectories is visible for many knickpoints when
251 they are close to the divide, for $nDD > \sim 0.8$ (Figure 8), which indicates that they slow down as they
252 approach the divide. The opposite is observed for some knickpoints when they are close to the outlet,
253 for $nDD < \sim 0.2 / 0.3$, with some trajectories suggesting, on the contrary, an acceleration after their
254 initiation ([Fig. 8](#); see also [Fig. 7](#)). These qualitative interpretations are supported by the detail analysis
255 of retreat velocity data shown in Figure 9. For each experiment, we show in Figure 9A the stack of
256 successive retreat velocities of each individual knickpoint according to distance nDD. [These data show](#)
257 [that the range of knickpoint retreat rates depends on the rate of base-level fall. Moreover, the envelopes](#)
258 draw a bell-shaped distribution for each experiment, which suggests [that retreat velocities are maximum](#)
259 when knickpoints are located at a mid-distance between the outlet and the divide, for central values of
260 nDD, between 0.4 and 0.6. This is supported by summary statistics of retreat velocities at 0.1 intervals
261 of nDD considering all knickpoints in each experiment (Fig. 9B). [Both the mean and median values](#)
262 show higher rates of upstream propagation when knickpoints are in the central section of rivers in the
263 three experiments, and conversely lower rates near the outlet ($nDD < 0.2 / 0.3$) where they initiate and
264 start to propagate and near the divide ($nDD > 0.8$), as suggested by trajectories shown in Figure 8. [To](#)

Supprimé: considering

Supprimé: Figure

Supprimé: Figure

Supprimé: T

Supprimé:

Supprimé:

Supprimé: Note that because knickpoint retreat rates also depend on the rate of base-level fall, the range of retreat rates is smaller in experiment with the lower rate of base level fall, BL05, so that their variation with distance is not as well defined as in both other experiments. However, the mean and median values are also slightly higher for intermediate distances which suggests that the trends described for the other two experiments are also valid here.

279 [further characterize this trend, we determined the position of maximum knickpoint velocity on](#)
280 [longitudinal profiles, hereafter \$nDD_{V_{max}}\$, from a second order polynomial fit \(Fig. 9C\). \$nDD_{V_{max}}\$ values](#)
281 [are very similar between experiments \(0.52, 0.57 and 0.54; Table 1\). They separate positive to negative](#)
282 [trends of knickpoint velocities versus normalized distance as also illustrated in Figure S4 \(see](#)
283 [Supplemental Material\).](#) Data from the three experiments indicate that after their initiation near the
284 outlet, knickpoints first speed up with a maximum in the central part of the catchments before
285 decelerating near the divide. It is worth noting that this specific trend of knickpoint retreat rates is
286 observed regardless of the experiment stages and thus whatever the position of the divide in the box.
287 This applies both to rivers in the early stages of experiments evolution, i.e. when they are small as well
288 as for very large rivers at the end of experiments. ▼

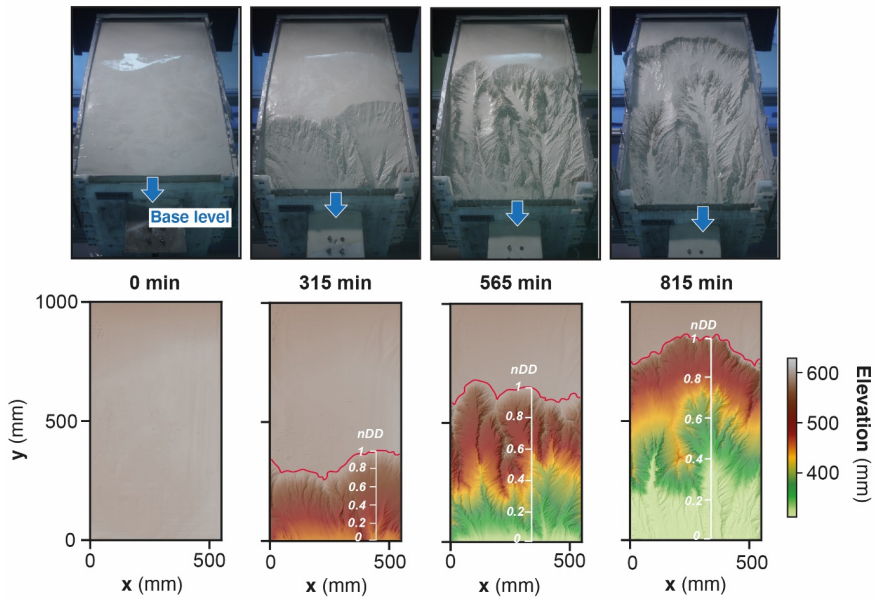
Supprimé: To further characterize this trend, we determined the position of maximum knickpoint velocity on longitudinal profiles, hereafter $nDD_{V_{max}}$, from a second order polynomial fit (Fig. 9C). This value is very similar between experiments, of 0.52, 0.57 and 0.54 (Table 1).

289

290

291

292



298

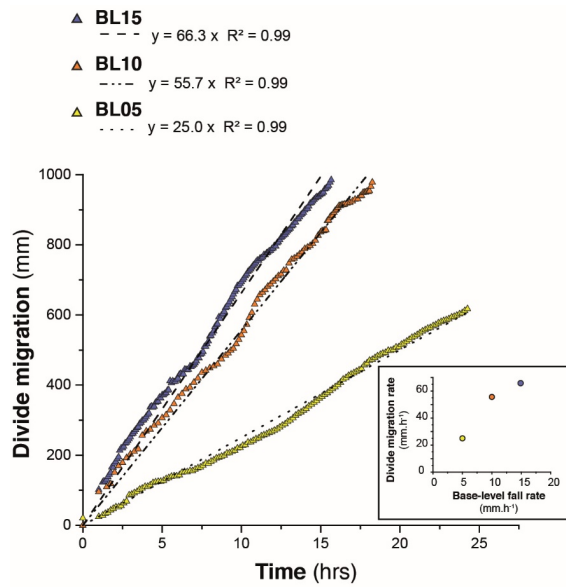
299 **Figure 4.** Photos (top row) and corresponding DEMs (bottom row) of experiment BL15 at four runtimes.

300 Note the propagation of the divide (red line) through the erosion box and the drop of the sliding gate
 301 used for falling base-level (blue arrows). The normalized distance to divide (nDD, see text) used to
 302 follow the position of knickpoints during runs is shown superimposed to DEMs.

303

Supprimé: (red line)

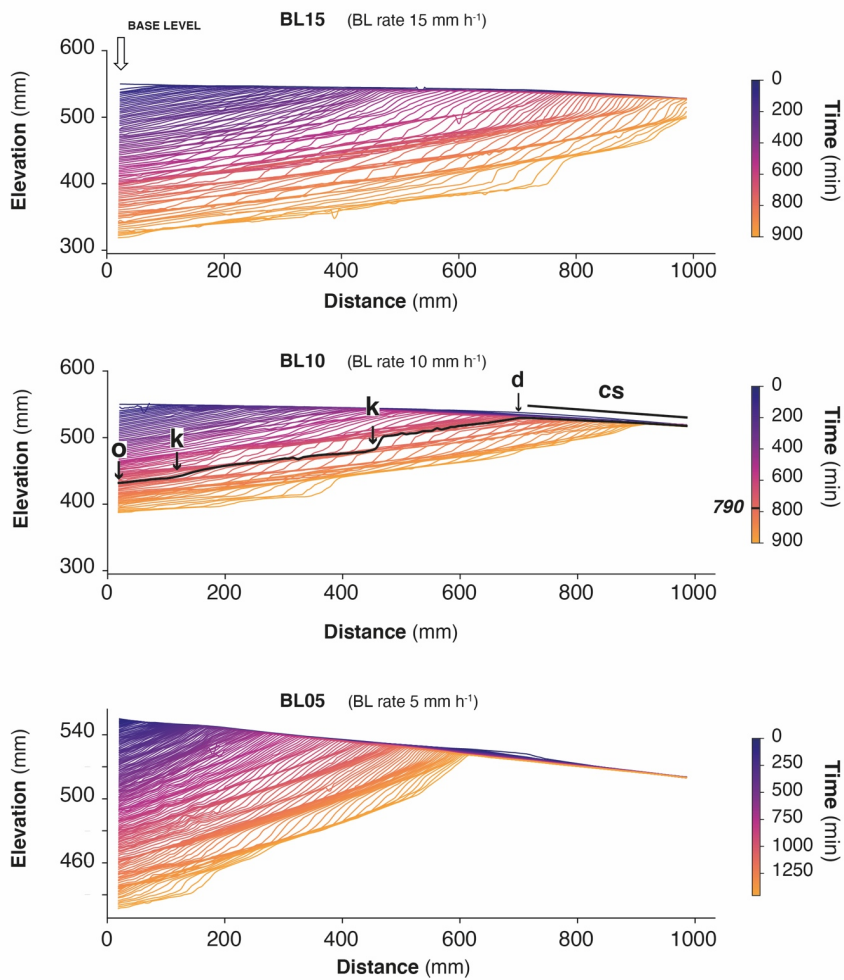
Supprimé: .



306

307 **Figure 5.** Evolution of the water divide position within the erosion box for the three experiments. The
 308 inset figure (Bottom right) shows the relation between the divide migration rate in the three experiments
 309 and their related base-level fall rate.

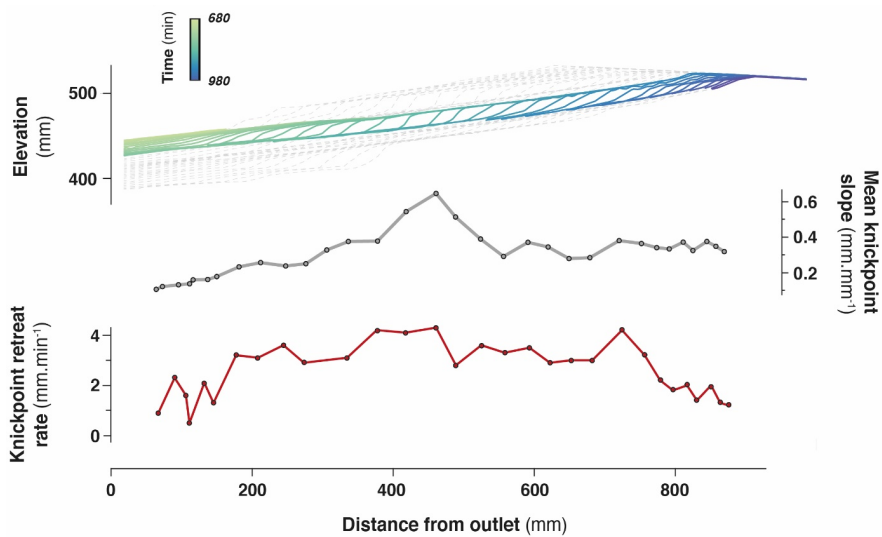
Supprimé: show



311

312 **Figure 6.** Successive river longitudinal profiles of experiments, shown here every 10 min. Each
 313 longitudinal profile is colored according to experimental runtime. The sliding gate used to drop the base
 314 level is to the left. Note the initial counterslope (cs). Black thick line on BL10 is the longitudinal profile
 315 at $t=790$ min, illustrating the outlet (o), knickpoints (k), and water divide (d). Note the change of scale
 316 for experiment BL05.

Supprimé: 790'

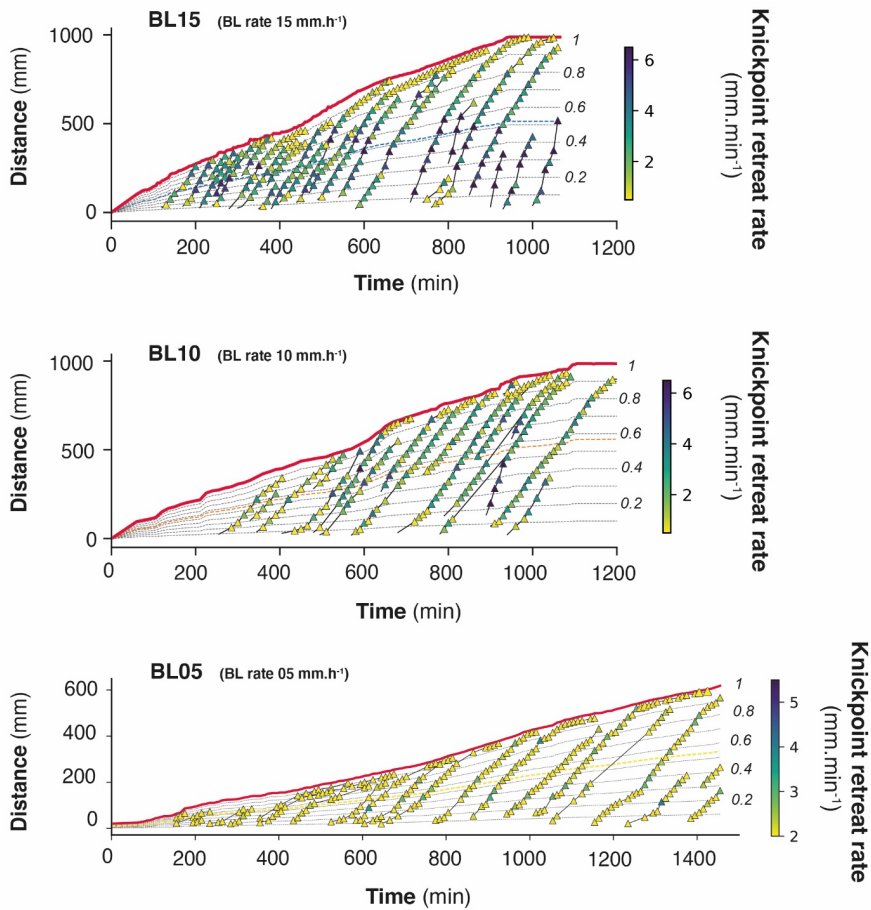


318

319 **Figure 7.** Retreat of an individual knickpoint from experiment BL10 (see also Fig. 6) showing its
 320 initiation with a gentle slope which subsequently steepen as it migrates upstream, (see also Fig. S3 in
 321 the Supplemental Material). Its maximum slope is reached at mid-distance between the outlet and the
 322 divide. Its lowest retreat rates are observed downstream near the outlet and upstream near the divide.

Supprimé: Detail r

Supprimé: .

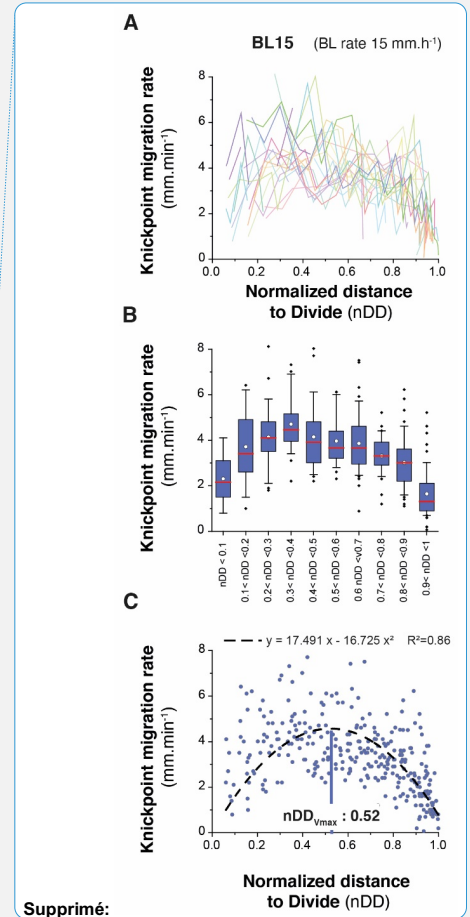
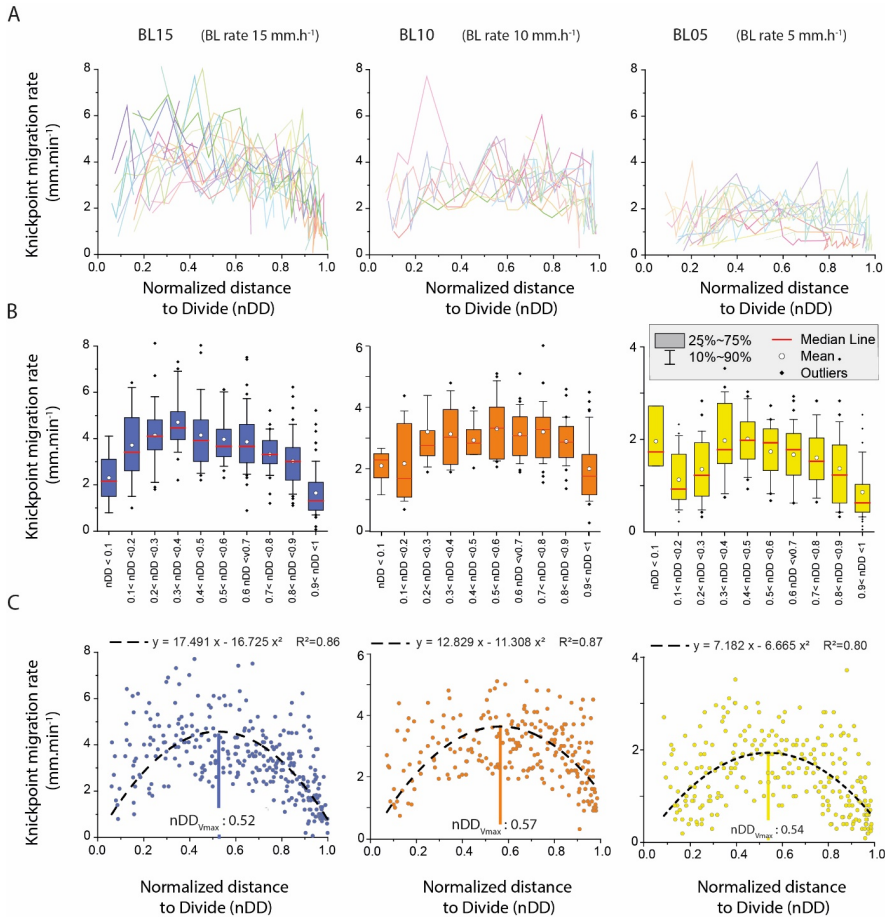


325

326

327 **Figure 8.** Space-time diagrams showing the propagation of the water divide (red line) and successive
 328 trajectories of knickpoints (triangles). Symbols color shows instant (10 min) knickpoints retreat rate.
 329 Thin black dashed lines show the normalized distances to divide (nDD). Thin colored dashed lines show
 330 $nDD_{V_{max}}$, the normalized distance where the highest rate of retreat velocity is deduced from the analysis
 331 (see text and Figure 9C). Note the change of scale and color bar for experiment BL10.

332



Supprimé:

Supprimé:).

333
 334 **Figure 9.** (A) Knickpoint retreat rates according to the normalized distances to divide (nDD) for each
 335 knickpoint of experiments. Each color line corresponds to an individual knickpoint of the space-time
 336 diagram in Fig. 8. *Note that the scale on the y-axis is the same for all graphs.* (B) Summary statistics of
 337 retreat rates for nDD intervals of 0.1. *Note the change in scale on the y-axis between the graphs.* (C)
 338 Plot of all knickpoints retreat rates for each experiment. *Note the change in scale on the y-axis between*
 339 *the graphs.* Black dashed line shows the second order polynomial fit to the data used to define the
 340 normalized longitudinal distance of maximum velocity of knickpoints (nDD_{vmax} ; see also Fig. S4 in the
 341 [Supplemental Material](#)).

3.2 Knickpoints initiation

To illustrate how knickpoints initiated near the outlet, we consider here a 120 minute-long sequence of channel evolution in experiment BL15 during which two knickpoints (K1 and K2) successively initiate and propagate upward (Fig. 10). In addition, we analyzed the history of channel width (Fig. 11A) and unit water discharge (Fig. 11B) at a cross-section located at 8 cm from the outlet (see location on Fig. 10B). We also present a summary of the statistics of normalized elevation changes (Fig. 11C) and shear stress (Fig. 11D) for all pixels across the section. The sequence starts with a “standard” profile (i.e., a typical river profile without any perturbation), at runtimes 880 and 890 min once a previous knickpoint had already propagated through the section, still visible upstream in Figure 10A. The channel is 23 to 25 mm wide (Fig. 10B and 11A) and the unit discharge is about $1.5 \cdot 10^6 \text{ mm}^2 \text{ h}^{-1}$. Erosion in the channel is on average lower than the base level fall as normalized erosion (erosion rate / base level fall rate) is < 1 for most pixels along the section (Fig. 11C). Then, the knickpoint K1 initiates at runtime 895 min and starts to propagate upstream. At the surveyed section, the channel first narrows, up to ~15 mm wide at 905 min (~60 % decrease), and then widens (~25 mm) once the knickpoint has moved upstream of the section, at 910 min (Fig. 10B). The narrowing phase is naturally associated with an increase of the unit discharge (Fig. 11B) and with enhanced erosion greater than the base level fall rate, up to 4 times the base level fall rate in average at 900 min (Fig. 11 C), with extremes as high as 8 times the base level fall rate. Once knickpoint K1 has retreated, unit discharge decreases as the channel subsequently widens, to reach a width of 25 cm to 28 cm between 925 and 930 min (Fig. 11A) while a new regular profile, i.e. without any slope break, established at 930 min (Fig. 10A). The normalized erosion across the section decreases below the base level value (Fig. 11C), with mean erosion rate values of 0.53, 0.36 and 0.76 times below the base level rates between 915 to 925 min. Longitudinally, the profiles stack together downstream of the knickpoint following its retreat from 895 to 925 min (Fig. 10A), which also indicates minor vertical erosion here once the knickpoint has retreated despite the ongoing base level falling. The second knickpoint (K2) then initiates at 935 min, propagates upstream in a similar way, leading to the setting up of a new regular profile at 980 min downstream its position at that time (Fig. 10A). Channel narrowing is also observed on the cross-section at the passage of this second knickpoint with a width

Supprimé: ¶

Supprimé: minutes

Supprimé: .

Supprimé: mm^3 .

Supprimé: mm^{-1} .

Supprimé:

Supprimé: 895'

Supprimé: section#

Supprimé: an

Supprimé: well above

Supprimé: this

Supprimé: this

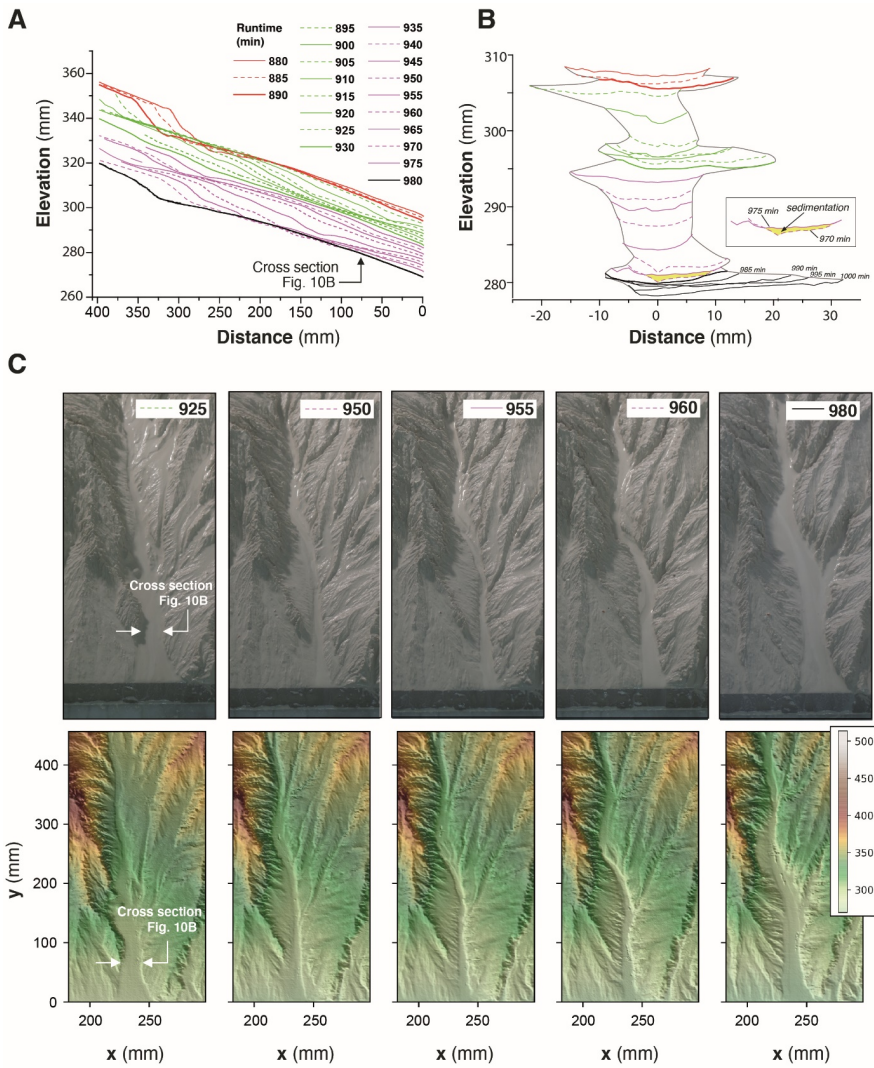
Supprimé: and disappears

Supprimé: (Fig.

389 that decreases to ~15 mm wide (Fig. 10B and 11A), associated with an increase of the unit discharge
390 and the erosion rate (Fig. 11C). It is followed again by a phase of widening to reach a width to around
391 30 / 35 mm once the knickpoint has propagated upstream and by a decreasing erosion below the base
392 level fall rate (Fig. 11C). Again, the longitudinal profiles stack together downstream of the knickpoint
393 (Fig. 10A). Note that at 975 min, most of the surveyed section is undergoing sedimentation (mean
394 normalized erosion rate is 0.1 and median is -0.25: Figures 10B and 11C). The distribution of river bed
395 shear stress along the section is given in the Figure 11D. Despite a large variability along the section,
396 one can observe a significant increase of the median and maximum values at the time of the knickpoint
397 passage, both for K1 and K2. Once knickpoints passed, the shear stresses decrease as the river widens.

398 This sequence illustrates that the rivers are never in equilibrium at the 5 min time-scale, but continuously
399 oscillate over time between disequilibrium states with periods when channel are too wide to keep pace
400 with the base level, and periods of knickpoint propagation when the erosion is enhanced to catch up the
401 base level. The river width is the regulation parameter which allows the river erosion to adapt
402 by increasing or decreasing the unit discharge. These knickpoints then propagate upward up to the divide
403 as discussed previously (Fig. 6). The average erosion rate is similar to the [base level](#) fall rate (mean
404 [normalized erosion rate of the sequence is 0.99](#)) but it does not correspond to any stable configuration
405 of the river since the erosion rate fluctuates between smaller and larger values. Knickpoints are by-
406 products of this unsteady dynamics, which are generated during the phases when the river catches up
407 with its erosion deficit with respect to the base level.

Supprimé: [baselevel](#)



409

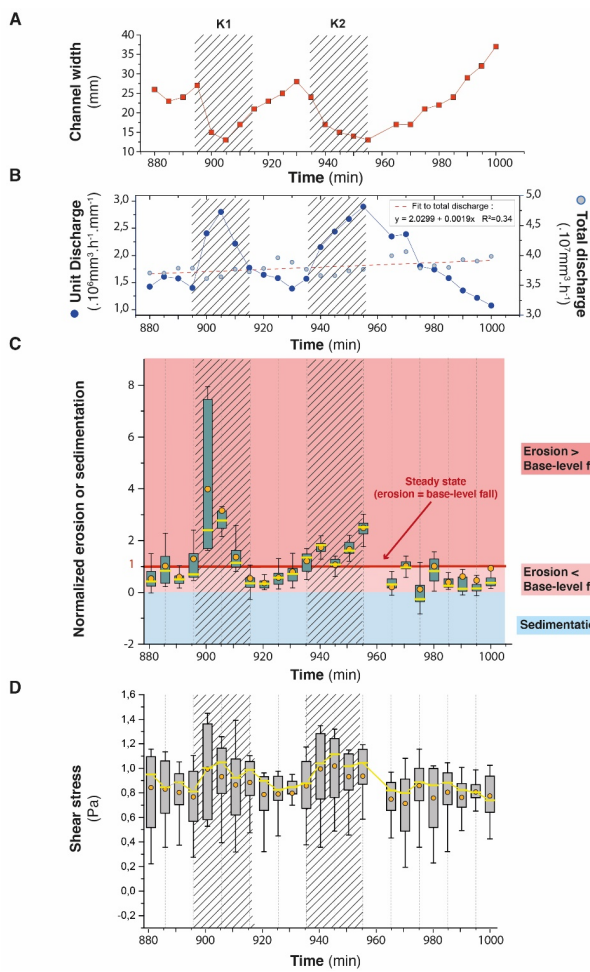
410 **Figure 10.** Downstream knickpoints initiation and propagation in a 120 *minute*-long sequence of
 411 experiment BL15 from experimental runtime 880 to 1000 minutes. (A) Sequence of downstream
 412 longitudinal profiles (5 min time-interval) of the investigated river, corresponding to the sequence
 413 hydro-geomorphic parameters shown in Figures 11 and 12. Propagation of the first (K1; initiated at
 414 895') and second (K2; initiated at 935') knickpoints is shown in green and purple colors respectively

Supprimé: minutes

416 (see text). (B) Time evolution of successive cross-sections of the channel at 80 mm from the outlet. Colors
 417 are the same as in Fig. 10A. (C) Photos (top row) and perspective views of DEM (bottom row) at five
 418 time-steps. Color bar is elevation in mm.

419

420



421

422 **Figure 11.** Time-series (5 min time interval) of river width (A) and unit and total discharge (B) for the
423 channel in experiment BL15 shown in Figure 10B, (see also location of Fig. 10C). Time-series of box-
424 and-whisker plots of normalized erosion or sedimentation (C) and shear stress (D) for all pixels across
425 the channel cross-section. Orange solid circles and yellow lines show the mean and median values,
426 respectively. Edges of the boxes indicate the 25th and 75th percentiles. Note that in C, normalized values
427 of 1 indicate erosion at the same rate as base-level fall (steady-state conditions). Values > 1 or <1
428 indicate respectively higher and lower erosion rate than BL fall rate. Negative values indicate
429 sedimentation. On all graphs, crosshatched areas indicate the passage of knickpoints K1 and K2.

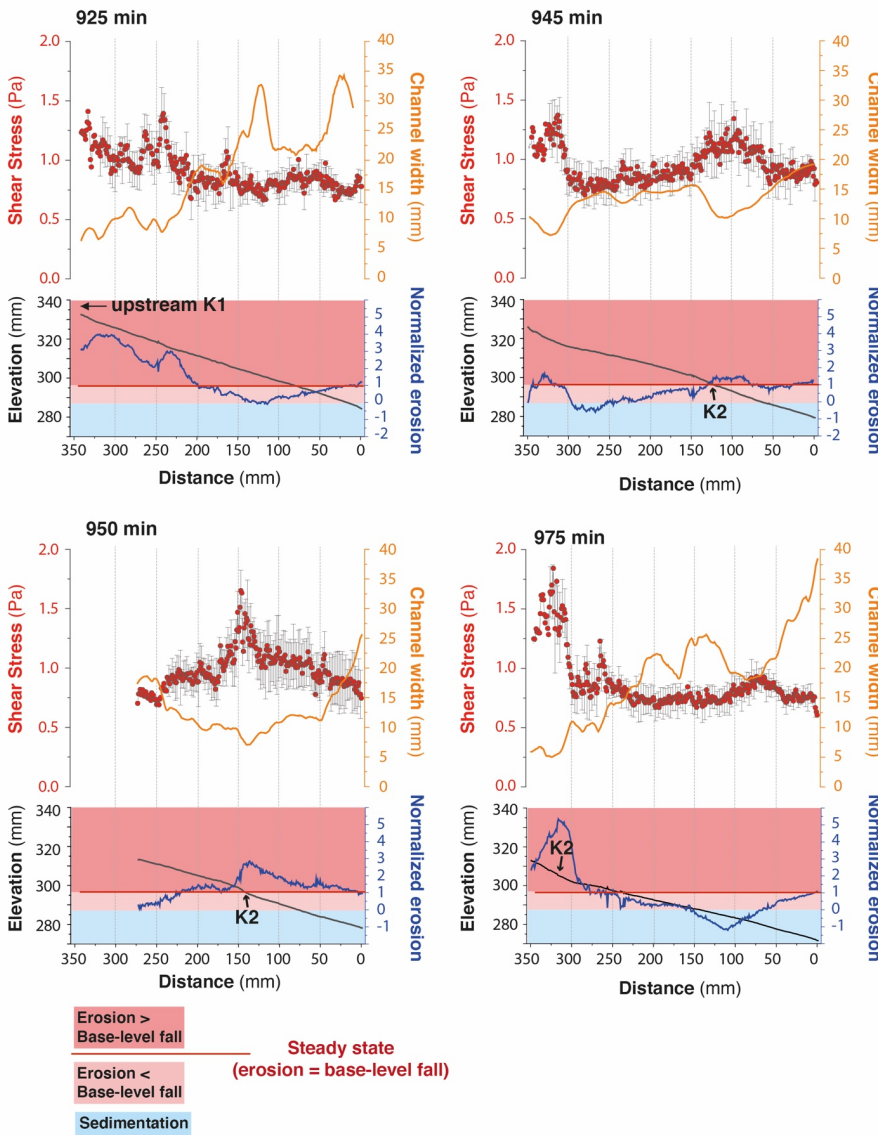
430 To complement cross-section data, we also illustrate (Fig. 12) how parameters vary longitudinally by
431 considering four stages, two before (925 min) and after (975 min) the passage of the knickpoint K2 and
432 two during its retreat (945 and 950 min). Note that at 925 min, the previous knickpoint (K1) has just
433 passed upstream the investigated profile and is responsible for the enhanced normalized erosion and
434 increased shear stress upstream between distance 200 to 350 mm. Similarly, at 975 min the second
435 knickpoint (K2) is still in the upstream part of the profile between distance 300 to 350 mm. We also
436 reported the longitudinal variations in river width, shear stress and normalized erosion along the profiles
437 (Fig. 12). At runtimes 925 and 975 min, before and after the passage of knickpoint K2, erosion is below
438 the base level rate along all the profiles down the knickpoints, with even localized sedimentation at 975
439 min between 50 and ~150 mm. These sections are characterized by low shear stress values, being
440 between 0.5 and 1 and by rivers that widen downward (around 0.7 mm/cm). On the opposite, during the
441 passage of knickpoint K2, at runtimes 945 and 950 min, mean shear stress increases locally at the
442 knickpoint location, being > 1 and the normalized erosion overpasses the base level rate there. These
443 knickpoint segments are characterized by a narrowing of the rivers as already shown previously. The
444 data illustrate that erosion mainly occurs during periods of knickpoint retreat though a combination of
445 local steepening of the profile and narrowing of the river, resulting in an increased shear stress. On the
446 opposite, once a knickpoint has propagated and between the passage of two successive knickpoints,
447 erosion decreases significantly and does not longer compensate the base level fall. These periods of
448 defeated erosion are characterized by low bed shear stress values in wide rivers, that widen downward.

Supprimé: .

Supprimé: than

Supprimé: and then

Supprimé: .



453

454 **Figure 12.** Longitudinal trends of hydro-geomorphic parameters in experiment BL15 at runtimes 925,
 455 945, 950 and 975 min (see text for comments). K1 and K2: first and second knickpoints discussed in the
 456 text (see also Fig. 10A).

457 **4 Discussion**

Supprimé: ¶

458 **4.1 Autogenic knickpoints**

459 Our experiments illustrate the generation and retreat of successive knickpoint waves that traveled across
460 the landscape during the growth of drainage networks. They formed throughout the duration of
461 experiments independent of the steady precipitation and base level fall rates and of the homogeneity of
462 the eroded material. These knickpoints were autogenically generated (Hasbargen and Paola, 2000),
463 arising only from internal geomorphic adjustments within the catchments rather than from variation in
464 external forcing. Our observations appear very similar to those of Hasbargen and Paola (2000, 2003)
465 and Bigi et al. (2006) who also reported the generation of successive autogenic knickpoints in landscape
466 experiments evolving under steady forcing (rainfall and base level fall rate) throughout the duration of
467 the runs. Unlike our experiments, which mainly consider the growth phase of drainage networks,
468 experiments reported in Hasbargen and Paola (2000, 2003) and Bigi et al. (2006) considered the
469 propagation of knickpoints after the phase of network growth, while their system was at steady-state on
470 average (mean catchment erosion rate equal to base level rate). Then, given that the size of their
471 experimental catchment was steady over time and given the steady rainfall rate, they were able to rule
472 out variations of water discharge over time as a main driver for the generation of their knickpoints. On
473 the opposite, in our experiments the size of catchments continuously increased over time, and thus the
474 water discharge. However, this does not appear as a key factor controlling knickpoints initiation for
475 several reasons. First, as we already mentioned, knickpoints arose at all stages of network growth and
476 divide retreat, for both small and large rivers (Fig. 8), and thus whatever the range of water discharge at
477 outlet. Second, the migration of the water divide related to drainage network growth occurred steadily
478 and roughly at a constant rate during the experiments (see Figures 5 and 8), as well as the size of the
479 catchments and the related increase in water discharge. Thus, we can rule out abrupt variations in
480 discharge as the driving mechanism for knickpoint initiation. Last, knickpoint initiations occurred at a
481 higher frequency than the increase in water discharge that resulted from catchment expansion and divide
482 migration. For example, in addition to unit discharge, we also reported on Figure 11B the variation in
483 total discharge during the 120 min-long sequence of knickpoint initiation discussed previously. The total

Supprimé: regardless

Supprimé: steadiness of the

Supprimé: equals

Supprimé: Then

489 discharge rose from $3.7 \cdot 10^7$ to $4.0 \cdot 10^7 \text{ mm}^3 \cdot \text{h}^{-1}$ in 120 minutes representing a $\sim 8\%$ increase, which is
490 relatively low compared to the $\sim 100\%$ increase of unit discharge during the passage of a knickpoint.
491 For all these reasons we conclude that the change in catchment size was not the main driver of successive
492 knickpoints initiation in our experiments, which occurred at a higher frequency.

Supprimé: .

493 4.2 Processes controlling knickpoints initiation and propagation

494 Given that the initiation of successive knickpoints was not related to changes in external factors and
495 catchment size over time, we consider internal geomorphic processes as driving mechanisms. The
496 detailed sequence of [knickpoint](#) initiation and propagation discussed above shows enhanced incision
497 above the rate of base level fall during the periods of knickpoints propagation. This occurred through
498 local steepening of the longitudinal profile and narrowing of the river, these two factors [lead](#) to an
499 increase in unit discharge and bed shear stress along the knickpoints. Several studies already
500 documented how steepening and narrowing act together for increasing river incision rate (e.g. Lavé and
501 Avouac, 2001; Duvall et al., 2004; Whittaker et al., 2007; Cook et al., 2013), which is what we also
502 document here. The novelty in our finding here, however, lies in the [evolution after](#) knickpoint retreat.

Supprimé: knickpoints

Supprimé: leading

503 [Immediately](#) after the retreat of a knickpoint, we show that erosion [in the section of the channel where](#)
504 [the knickpoint just passed](#) is inhibited despite the ongoing [base level fall: river incision is lower than the](#)
505 [rate of](#) base level fall, until the passage of a new knickpoint. Although only illustrated in the sequence
506 detailed previously (Figs. 10 to 12), this was a general behavior that [occurred in all](#) three experiments
507 [along](#) their whole longitudinal profile, not only their downstream part as in this sequence. [This](#)

Supprimé: phase of post-

Supprimé: Actually, immediately

Supprimé: downstream and rivers no longer incised

Supprimé: concerned the

Supprimé: and

Supprimé: Actually, this

508 systematic decrease in erosion downstream of the knickpoints is inherent to the geometry of the stacks
509 of all successive longitudinal profiles of each experiment (Fig. 6). In most cases, profiles downstream
510 of retreating knickpoints stack on top of each other, as illustrated schematically on Figure 13A, which
511 indicates minor or no erosion downstream of the knickpoints until the passage of a new one. In the case
512 of continuous [steady](#) adjustment of rivers to base level fall downstream of the knickpoints, the geometry
513 of profiles should [instead](#) show a pattern as illustrated in Figure 13B. The pattern of profiles evolution
514 over time documented here is usually observed following incremental drops in base level (Finnegan,
515 2013; Grimaud et al., 2016) and to our best knowledge this is the first time here that such geometry is

Supprimé: rather

526 documented in the case of a continuous base level fall. This particular pattern is explained by the
527 decrease in erosion rate downstream of the retreating knickpoints which acts as if the base level was not
528 falling continuously at a constant rate but instead dropped regularly step-by-step. Therefore,
529 understanding the systematic occurrence of successive knickpoints in our experiments requires
530 understanding why erosion rate dropped downstream of knickpoints, following their retreat. After the
531 passage of knickpoints, we systematically observe a widening of the rivers, as also documented in
532 natural systems (e.g. Cook et al., 2014; Zavala-Ortiz et al., 2021) and a decrease in the bed shear stress.
533 Because an increase in channel width over time inevitably reduces the bed shear stress if discharge and
534 river gradient remain constant (Fuller et al., 2016), we propose that widening was the main factor
535 responsible for the decrease in shear stress and erosion rate after the passage of a knickpoint, and thus
536 for the occurrence of the successive autogenic knickpoints. Demonstrating the sole effect of river width
537 on bed shear stress and erosion rate is complicated by covariations of these factors with river slope and
538 variations of discharge related to connection of tributaries. This can be illustrated however on the basis
539 of the sequence considered previously, particularly at runtime 925 min between the passage of the two
540 successive knickpoints K1 and K2 (Figs. 10 and 12). At that time, the profile of the river here had a
541 roughly constant slope (Fig. 14), without any slope break and no major tributary connected (Fig. 10)
542 that could have significantly changed the water discharge. As illustrated in Figure 12, this river segment
543 was characterized by widening and decreasing shear stress downward despite constant slope and total
544 discharge. Thus, this example illustrates a decrease in shear stress that was only the result of the
545 widening of the river downward (Fig. 14), which supports the hypothesis that decreased erosion
546 downstream of the propagating knickpoints was mainly due to the widening dynamics of the
547 experimental rivers.

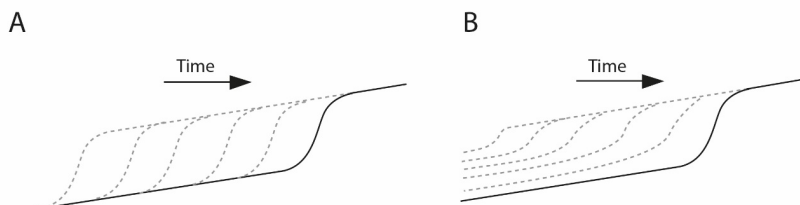
Supprimé: finally

Supprimé: to understand

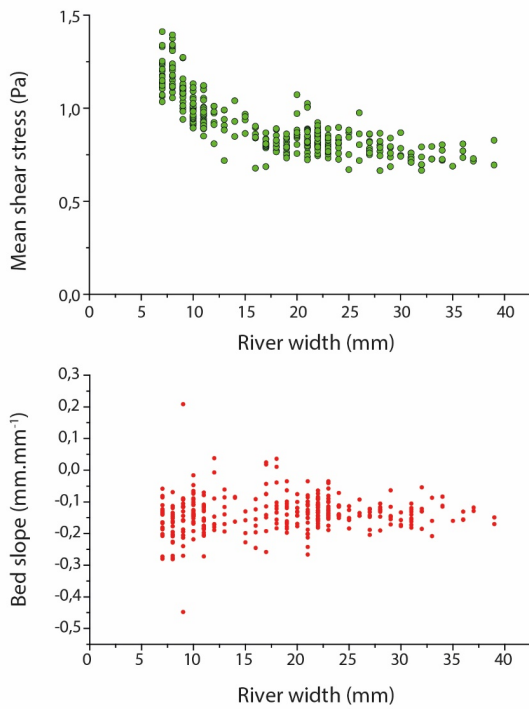
Supprimé: then

Supprimé: Then

Supprimé: defeated



554 **Figure 13.** Sketches illustrating the difference in the geometry of successive longitudinal profiles
 555 following the retreat of a knickpoint depending on whether fluvial incision is inhibited (A) or not (B)
 556 downstream of the retreating knickpoint with respect to the continuously falling base level.



557

558 **Figure 14.** Top: river bed shear stress versus river width in the downstream section, 40 cm-long, of
 559 experiment BL15 at runtime 925 (see also Fig. 12). Bottom: corresponding slope of the river bed.

560

561 Incision of rivers in our experiments is fundamentally discontinuous despite continuous forcing and we
 562 highlight downstream river width dynamics, in particular river widening, as a main cause of instability.

563 We show that once knickpoints have retreated, unit discharge, shear stress and incision rate all decrease

564 downstream while the rivers widen, resulting in a state where incision no longer counterbalances the
 565 base-level fall. This results in an unstable situation that ends with the initiation and propagation of a new

Supprimé: according to

Supprimé: counterbalance

Supprimé: up

569 knickpoint and a new sequence of width narrowing, increasing shear stress and incision rate, allowing
570 the river to recover from the incision delay accumulated during the previous widening period. Further
571 work is required to understand the mechanisms responsible for lateral channel erosion in our
572 experiments, which is a key ingredient for understanding river mobility and widening. Several field (e.g.
573 Hartshorn et al., 2002; Turowski et al., 2008; Fuller et al., 2009), experimental (e.g. Wickert et al., 2013;
574 Bufe et al., 2016; Fuller et al., 2016; Baynes et al., 2020) and numerical (e.g. Turowski et al., 2007;
575 Lague, 2010; Langston and Tucker, 2018; Li et al., 2021) studies have demonstrated that high sediment
576 flux relative to transport capacity promotes increased lateral channel erosion. Most of these studies
577 highlight the role of cover effect, the protection of the river bed by transient deposition of sediments on
578 the river bed (Sklar and Dietrich, 2001; Turowski et al., 2007, 2008; Lague, 2010; Baynes et al., 2020;
579 Li et al., 2021), as a main factor promoting lateral erosion in high sediment flux settings. Other studies
580 show that by modifying the bed roughness, sediment deposition may deflect the flow, which also
581 promotes lateral erosion and widening (Finnegan et al., 2007; Fuller et al., 2016). Contrary to
582 experimental devices specifically designed to address these issues (e.g. Finnegan et al., 2007; Fuller et
583 al., 2016), direct observation on actual processes that drive lateral erosion in our experiments is made
584 difficult by the small size of the topographic features, the depth of rivers being of millimeter scale, and
585 by the low grain size of the material used. Opacity due to the generation of the artificial rainfall also
586 considerably limits direct observation during the runs. Despite these limitations, data suggest that lateral
587 erosion and river widening in our experiments is also related to [an](#) increase in sediment flux. We show
588 [that knickpoints are locations](#) of enhanced erosion well above the rate of base level fall. We document
589 for example, mean erosion rates greater than 5 times the base level fall rate, with extreme values up to
590 a factor of 8 locally (Fig. 11 and 12). Downstream, where rivers widen, we observe that the general
591 decrease in erosion rate is also associated with local deposition in some parts of the channels (for
592 example at runtime 915 min in Figure 11 or 975 min in Figures 10 to 12). We [thus](#) hypothesize that
593 lateral erosion and widening are due in part to the increase sediment flux related to enhanced erosion on
594 knickpoints. Further work is needed to test this hypothesis, for example by investigating in detail spatio-
595 temporal variations in erosion and sedimentation during width widening.

Supprimé: , large flumes in particular

Supprimé: actually

Supprimé: location

Supprimé: then

600 Further work is also needed to better understand how knickpoints initiate after the phases of widening,
601 in particular for determining whether river narrowing drives the formation of the knickpoints (e.g. Amos
602 and Burbank, 2007) or whether narrowing is a consequence of steepening (e.g. Finnegan et al., 2005).
603 Some studies that investigated river response to increased uplift rate show that narrowing alone, at
604 constant river gradient, can allow rivers to increase their incision rate (Lavé and Avouac, 2001; Duvall
605 et al., 2004; Amos et al., 2007). In this context, Amos et al. (2007) propose a model in which the river
606 response to an increase in uplift rate first involves width narrowing, with the increase in slope and
607 formation of a knickpoint occurring only in a second stage, if the increase in incision induced by
608 narrowing is not sufficient to counteract the uplift rate. In our experiments here, we suggest that channel
609 narrowing predates, and in fact enables, the steepening of the profile in the initial stages of knickpoints
610 formation. Indeed, we observe that the transition from a wide to a narrow channel occurs very quickly,
611 at a smaller time scale than the time interval between two successive digitization of the experiments (5
612 min), and the knickpoints that form then have a very gentle slope, which then amplifies as they migrate
613 upstream (Fig. 7). This suggests that it is not the steepening that drives river narrowing but on the
614 contrary that narrowing is essential for knickpoints to initiate. Further work would also be needed to
615 verify this hypothesis, in particular with additional experiments with much higher frequency of data
616 acquisition to capture these changes in much more detail.

617 4.3 Implications

618 Knickpoints in river longitudinal profiles are commonly related to variations in tectonics or climate
619 through their influence on base level and/or sediment supply (e.g. Whipple and Tucker, 1999; Crosby
620 and Whipple, 2006; Kirby and Whipple, 2012; Whittaker and Boulton, 2012) and are then used to
621 highlight such changes when interpreting their occurrence in natural systems. The recognition here that
622 knickpoints may be generated autogenically due to cycles of river widening and narrowing is then of
623 first importance for retrieving information on tectonics and climate from their record in landscapes in
624 the form of knickpoints. Finding criteria that could be used in the analysis of natural systems to
625 differentiate these autocyclic knickpoints from those formed in response to tectonics or climate would
626 be an important step in the continuation of this work. A specificity of knickpoints in our experiments is

Supprimé: ¶

Supprimé: the rivers

629 to initiate downstream with a gentle slope, which subsequently steepen in the early stages of migration,
630 and as a hypothesis we suggest that this may be characteristic of their autogenic formation following the
631 mechanism described here. Being able to recognize these autogenic knickpoints would also be important
632 for studies that investigate knickpoints propagation (e.g. Crosby and Whipple 2006; Berlin and
633 Anderson, 2007; Schwanghart and Scherler, 2020) because knickpoints in our experiments are
634 characterized by an upward dynamic of retreat that is not conventional. According to stream-power
635 based celerity models, these studies consider that the upstream propagation rate of knickpoints depends
636 inversely on drainage area (a proxy for discharge; Crosby and Whipple 2006; Berlin and Anderson,
637 2007), implying a monotonous decrease of their retreat rate as they propagate upstream due to the
638 progressive reduction of drainage area and water discharge. This property is used for example to invert
639 their present location for dating the external perturbation responsible for their formation (Crosby and
640 Whipple 2006; Berlin and Anderson, 2007). Here, knickpoints in our experiments first accelerate during
641 their initial stages of propagation before decelerating in a second time as they approach the divide
642 (Fig.9). Only this later phase of decreasing knickpoint velocity in the upstream part of rivers (for
643 normalized distance $NDD > nDD_{v_{max}}$: Fig. 9) is consistent with predictions from stream-power based
644 celerity models (see Fig. S5 in the Supplemental Material). On the opposite, a sole control by drainage
645 area and discharge cannot explain the increase in velocity observed in the downstream sections (for
646 $NDD < nDD_{v_{max}}$: Fig. 9), which implies an additional controlling factor. We suggest that this specific
647 mode of retreat downstream is related to the progressive steepening of the knickpoints rather than to a
648 purely hydrologic control. Deciphering the respective roles of slope and discharge in the retreat
649 dynamics documented would require further in-depth analysis, particularly during the early stages of
650 initiation and propagation which appear to be specific to the autogenic mechanism defined here.

651 We show that the formation of knickpoints in our experiments is closely related to periods of decreasing
652 erosion rate as the rivers widen, counterbalanced by increasing rate greater than the rate of base level
653 fall as the rivers narrow and knickpoints form. Thus, the sequential evolution of longitudinal profiles is

654 very similar to the geometry that would be observed if the system was forced by discrete drops of the
655 base level, rather than by a continuous drop as it is actually the case. We did not measure the sediment

Supprimé: then amplifies

Supprimé: S3

Supprimé: more consistent with

Supprimé: base level

660 flux at the output of our models, but we can assume that it would be characterized by fluctuations
661 controlled by the frequency of knickpoint initiation, superimposed on a longer-term increasing trend
662 related to the growth of drainage networks. Some sediment outflux fluctuations were actually measured
663 by Hasbargen and Paola (2000) in their experiments and interpreted as the consequence of knickpoint
664 propagation. This study and our work illustrate that fluctuations in sediment flux can be observed at
665 catchments outlet despite constant forcing parameters, when autocyclic knickpoints are generated in
666 river systems.

667 By performing such exploratory experiments, we do not pretend to reproduce natural landscapes in the
668 laboratory because of important scaling issues (see Paola et al., 2009 for an extensive reflection on this
669 matter) but rather to highlight and document complex system behaviors under controlled conditions that
670 could provoke further investigations. Our findings support ongoing investigations that aim in better
671 understanding the links between lateral erosion, channel geometry and valley width which is an issue
672 that is emerging in the last years (e.g. Turowski, 2018; Croissant et al., 2019; Langston and Tucker,
673 2019; Baynes et al., 2020; Zavala-Ortiz et al., 2021). A perspective to our work would be to investigate
674 the mechanism of knickpoints generation driven by river width variations and the conditions that lead
675 to their formation using landscape evolution models that incorporate lateral erosion and a dynamic river
676 width (e.g. Davy et al., 2017; Carretier et al., 2018; Langston and Tucker, 2019). Simulations of
677 Langston and Tucker (2019) highlight the role of bedrock erodibility as an important factor controlling
678 lateral migration of rivers and the width of valleys, an issue that has not been investigated here given
679 the similarity of the eroded materials in our experiments here. This study also confirms the assumption
680 of Hancock and Anderson (2002) that lateral erosion and widening occurs preferentially in contexts of
681 low incision rate, *i.e.* in domains with low uplift rate. This is likely in such contexts that the new mode
682 of autogenic knickpoints formation driven by river width dynamics that we define in this study should
683 apply.

684 **5 Conclusion**

685 Knickpoints in the longitudinal profile of rivers are commonly assumed to be incisional waves that
686 propagate upstream through landscapes in response to changes in tectonics, climate or base-level. Based

Supprimé: considered as

688 on results from a set of laboratory experiments at the drainage basin scale that simulate the growth of
689 drainage networks in response to constant base level fall and rainfall, we show that knickpoints also
690 form autogenically, independent of any variations in these external forcing factors. In all experiments,
691 successive knickpoints initiate and propagate upward throughout the duration of the experimental runs,
692 independent of the rate of base level fall applied and of the size of the rivers as the catchments expand.
693 Thanks to the computation of hydraulic information (water depth, river width, discharge and shear
694 stress) using a hydrodynamic model, we show that the formation of knickpoints is driven by variations
695 in river width at the outlet of catchments and we highlight width widening as a main cause of instability
696 leading to knickpoint formation. Widening entails a decrease in shear stress and an incision rate lower
697 than the rate of base level fall, resulting in an unstable situation that ends up with a sequence of width
698 narrowing, increasing shear stress and incision rate as a knickpoint initiates. Rivers in our experiments
699 thus evolve following sequences of width widening and narrowing that drive the initiation and
700 propagation of successive knickpoints. As a result, incision is fundamentally discontinuous over time
701 despite continuous forcing. It occurs during discrete events of knickpoint propagation that allow, the
702 rivers to recover from the incision delay accumulated during widening periods.

Supprimé: independently

Supprimé: regardless

Supprimé: actually

Supprimé: s

703

704 **Author contributions.** SB designed the experimental device. LdL, SB and AG built the experimental
705 setup and carried out the experiments. LdL analyzed the data with the help of SB and PhD. All authors
706 discussed the data. LdL and SB wrote the manuscript with input from AG and PhD.

707

708 **Acknowledgements.** This work was supported by ORANO-Malvesi and CNRS-INSU Tellus-Syster
709 programme. We thank Sebastien Carretier and Odin Marc for fruitful discussions and Jens Turowski
710 for his comments on a preliminary version of this manuscript. We thank Laure Guerit and an
711 anonymous reviewer for their constructive comments which greatly improved the manuscript.

712

713 **References**

718 Amos, C.B., and Burbank, D.W.: Channel width response to differential uplift: *J. Geophys. Res.*, 112,
719 doi:10.1029/2006JF000672, 2007.

720 Baynes, E.R.C., Lague, D., Attal, M., Gangloff, A., Kirstein, L.A., and Dugmore, A.J.: River self-
721 organisation inhibits discharge control on waterfall migration: *Scientific Reports*, v. 8, p. 2444,
722 doi:10.1038/s41598-018-20767-6, 2018.

723 Baynes, E.R.C., Lague, D., Steer, P., Bonnet, S., and Illien, L.: Sediment flux-driven channel
724 geometry adjustment of bedrock and mixed gravel–bedrock rivers: *Earth Surface Processes and*
725 *Landforms*, v. 45, p. 3714–3731, doi:10.1002/esp.4996, 2020.

726 Berlin, M.M., and Anderson, R.S.: Modeling of knickpoint retreat on the Roan Plateau, western
727 Colorado: *Journal of Geophysical Research*, v. 112, p. F03S06, doi:10.1029/2006JF000553, 2007.

728 Bigi, A., Hasbargen, L.E., Montarani, A., and Paola, C.: Knickpoints and hillslope failure: Interactions
729 in a steady-state experimental landscape, *in* Willet, C.D., Hovius, N., Brandon, M.T., and Fisher,
730 D.M., eds. *Tectonics, Climate and Landscape evolution: Geological Society of America Special paper*
731 398, p. 295-307, doi:10.1130/2006.2398(18), 2006.

732 Bonnet, S.: Shrinking and splitting of drainage basins in orogenic landscapes from the migration of the
733 main drainage divide: *Nature Geoscience*, v. 2, p. 766–771, doi:10.1038/ngeo666, 2009.

734 Bonnet, S., and Crave, A.: Landscape response to climate change: Insights from experimental
735 modeling and implications for tectonic versus climatic uplift of topography: *Geology*, v. 31, p. 123–
736 126, doi: 10.1130/0091–7613, 2003.

737 Bufo, A., Paola, C., and Burbank, D.W.: Fluvial beveling of topography controlled by lateral channel
738 mobility and uplift rate: *Nature geosc.*, 9, 706-710, doi:10.1038/ngeo2773, 2016.

739 Cantelli, A., and Muto, T.: Multiple knickpoints in an alluvial river generated by a single drop in base
740 level: experimental investigation: *Earth Surface Dynamics*, 2, 271-278, doi:10.5194/esurf-2-271-2014,
741 2014.

742 Carretier, S., Godderis, Y., Maertinez, J., Reich, M., and Martinod, J.: Colluvial deposits as a possible
743 weathering reservoir in uplifting mountains: *Earth Surf. Dynam.*, 6, 217-237, doi: 10.5194/esurf-6-
744 217-2018, 2018.

745 Cook, K.L., Turowski, J.M., and Hovius, N.: A demonstration of the importance of bedload transport
746 for fluvial bedrock erosion and knickpoint propagation: *Earth Surface Processes and Landforms*, v. 38,
747 p. 683–695, doi:10.1002/esp.3313, 2013.

748 Cook, K.L., Turowski, J.M., and Hovius, N.: River gorge eradication by downstream sweep erosion:
749 *Nature geoscience*, doi:10.1038/NGEO2224, 2014.

750 Croissant, T., Lague, D., and Davy, P.: Channel widening downstream of valley gorges influenced by
751 flood frequency and floodplain roughness: *Journal of Geophysical Research-Earth Surface*, v. 124, p.
752 154–174, doi:10.1029/2018JF004767, 2019.

753 Crosby, B.T., and Whipple, K.X.: Knickpoint initiation and distribution within fluvial networks: 236
754 waterfalls in the Waipaoa River, North Island, New Zealand: *Geomorphology*, v. 82, p. 16–38,
755 doi:10.1016/j.geomorph.2005.08.023, 2006.

756 Davy, P., Croissant, T., and Lague, D.: A precipitation method to calculate river hydrodynamics, with
757 applications to flood prediction, landscape evolution models, and braiding instabilities: *J. Geophys.*
758 *Res.-Earth*, 122, 1491-1512, doi:10.1002/2016JF004156, 2017.

759 Davy, P., Croissant, T., and Lague, D.: A precipiton method to calculate river hydrodynamics, with
760 applications to flood prediction, landscape evolution models, and braiding instabilities: *Journal of*
761 *Geophysical Research-Earth Surface*, v. 122, p. 1491–1512, doi:10.1002/2016JF004156, 2017.

762 Duvall, A., Kirby, E., and Burbank, D.: Tectonic and lithologic controls on bedrock channel profiles
763 and processes in coastal California: *Journal of Geophysical Research*, v. 109, p. F03002,
764 doi:10.1029/2003JF000086, 2004.

765 Finnegan, N.J.: Interpretation and downstream correlation of bedrock river terrace treads created by
766 propagation knickpoints: *Journal of Geophysical Research-Earth Surface*, v. 118,
767 doi:10.1029/2012JF002534, 2013.

768 Finnegan, N.J., and Dietrich, W.E.: Episodic bedrock strath terrace formation due to meander
769 migration and cutoff: *Geology*, 39, 143-146, doi:10.1130/G31716.1, 2011.

770 Finnegan, N.J., Roe, G., Montgomery, D.R., and Hallet, B.: Controls on the channel width of rivers:
771 Implications for modeling fluvial incision of bedrock: *Geology*, 33, 229-232, doi:10.1130/G21171.1,
772 2005.

773 Fuller, T.K., Perg, L.A., Willenbring, J.K., and Lepper, K.: Field evidence of climate-driven changes
774 in sediment supply leading to strath terrace formation: *Geology*, 37, 467-470,
775 doi:10.1130/G25487A.1, 2009.

776 Fuller, T.K., Gran, K.B., Sklar, L.S., and Paola, C.: Lateral erosion in an experimental bedrock
777 channel: The influence of bed roughness on erosion by bed load impacts: *Journal of Geophysical*
778 *Research-Earth Surface*, v. 121, p. 1084-1105, doi:10.1002/2015JF003728, 2016.

779 Grimaud, J.-L., Paola, C., and Voller, V.: Experimental migration of knickpoints: influence of style of
780 base-level fall and bed lithology: *Earth Surface Dynamics*, v. 4, p. 11-23, doi:10.5194/esurf-4-11-
781 2016, 2016.

782 Hancock, G.S., and Anderson, R.S.: Numerical modeling of fluvial strath-terrace formation in
783 response to oscillating climate: *Geological Society of America Bulletin*, v. 114, p. 1131-1142, 2002.

784 Hartshorn, K., Hovius, N., Dade, W.B., and Slingerland, R.L.: Climate-driven bedrock incision in an
785 active mountain belt: *Science*, 297, 2036-2038, 2002.

786 Hasbargen, L.E., and Paola, C.: Landscape instability in an experimental drainage basin: *Geology*, v.
787 24, p. 1067-1070, 2000.

788 Hasbargen, L.E., and Paola, C.: How predictable is local erosion rate in erosional landscape ? *in*
789 Wilcox, P.R. and Iverson, R.M., eds., Prediction in Geomorphology: American Geophysical Union
790 Geophysical Monograph 135, doi:10.1029/135GM16, 2003.

791 Hilley, G.E., and Arrowsmith, J.R.: Geomorphic response to uplift along the Dragon's Back pressure
792 ridge, Carrizo Plain, California: *Geology*, v. 36, p. 367-370, doi:10.1130/G24517A.1, 2008.

793 Kirby, E., and Whipple, K.X.: Expression of active tectonics in erosional landscapes: *Journal of*
794 *Structural Geology*, v. 44, p. 54–75, doi:10.1016/j.jsg.2012.07.009, 2012.

795 Lague, D.: Reduction of long-term bedrock incision efficiency by short-term alluvial cover
796 intermittency: *J. Geophys. Res.*, 115, doi:10.1029/2008JF001210, 2010.

797 Lague, D., Crave, A., and Davy, P.: Laboratory experiments simulating the geomorphic response to
798 tectonic uplift: *Journal of Geophysical Research-Solid Earth*, v. 108, doi:10.1029/2002JB001785,
799 2003.

800 Langston, A.L., and Tucker, G.E.: Developing and exploring a theory for the lateral erosion of
801 bedrock channels for use in landscape evolution models: *Earth Surf. Dynam.*, 6, 1-27,
802 doi:10.5194/esurf-6-1-2018, 2018.

803 Lavé, J., and Avouac, J.P.: Fluvial incision and tectonic uplift across the Himalayas of central Nepal:
804 *Journal of Geophysical Research-Solid Earth*, v. 106, p. 26561–26591, doi:10.1029/2001JB000359,
805 2001.

806 Li, T., Venditti, J.G., and Sklar, L.S.: An analytical model for lateral erosion from saltating bedload
807 particle impacts: *J. Geophys. Res.– Earth*, 126, doi:10.1029/2020JF006061, 2021.

808 Mitchell, N.A., and Yanites, B.J.: Spatially variable increase in rock uplift in the Northern U.S.
809 Cordillera recorded in the distribution of river knickpoint and incision depths: *Journal of Geophysical*
810 *Research: Earth Surface*, v. 124, 1238-1260, doi:10.1029/2018JF004880, 2019.

811 Moussirou, B., and Bonnet, S.: Modulation of the erosion rate of an uplifting landscape by long-term
812 climate change: An experimental investigation: *Geomorphology*, v. 303, p. 456–466,
813 doi:10.1016/j.geomorph.2017.12.010, 2018.

814 Paola, C., Straub, K., Mohrig, D., and Reinhardt, L.: The “unreasonable effectiveness” of stratigraphic
815 and geomorphic experiments: *Earth-Science Reviews*, v. 97, p. 1–43,
816 doi:10.1016/j.earscirev.2009.05.003, 2009.

817 Rohais, S., Bonnet, S., and Eschard, R.: Sedimentary record of tectonic and climatic erosional
818 perturbations in an experimental coupled catchment-fan system: *Basin Research*, v. 24, p. 198–212,
819 doi:10.1111/j.1365-2117.2011.00520.x, 2012.

820 Scheingross, J.S., Lamb, M.P., and Fuller, B.M.: Self-formed bedrock waterfalls: *Nature*, v. 567, p.
821 229–233, doi:10.1038/s41586-019-0991-z, 2019.

822 Schwanghart, W.S., and Scherler, D.: Divide mobility controls knickpoint migration on the Roan
823 Plateau (Colorado, USA): *Geology*, 48, 698-702, doi:10.1130/G47054.1, 2020.

824 Singh, A., Reinhardt, L., and Foufoula-Georgiou, E.: Landscape reorganization under changing
825 climatic forcing: Results from an experimental landscape: *Water Resources Research*, v. 51, p. 4320–
826 4337, doi:10.1002/2015WR017161, 2015.

827 Sklar, L.S., and Dietrich, W.E.: Sediment and rock strength controls on river incision into bedrock:
828 *Geology*, 29, 1087-1090, 2001.

829 Sweeney, K.E., Roering, J.J., and Ellis, C.: Experimental evidence for hillslope control of landscape
830 scale: *Science*, v. 349, p. 51–53, doi:10.1126/science.aab0017, 2015.

831 Tofelde, S., Savi, S., Wickert, A. D., Bufe, A., and Schildgen, T. F.: Alluvial channel response to
832 environmental perturbations: fill-terrace formation and sediment-signal disruption. *Earth Surface*
833 *Dynamics*, v. 7, p. 609-631, doi:10.5194/esurf-7-609-2019, 2019.

834 Turowski, J.M.: Alluvial cover controlling the width, slope and sinuosity of bedrock channels: *Earth*
835 *Surface Dynamics*, v. 6, p. 29–48, doi:10.5194/esurf-6-29-2018, 2018.

836 Turowski, J.M., Lague, D., Crave, A., and Hovius, N.: Experimental channel response to tectonic
837 uplift: *Journal of Geophysical Research-Earth Surface*, v. 111, doi:10.1029/2005JF000306, 2006.

838 Turowski, J.M., Lague, D., and Hovius, N.: Cover effect in bedrock abrasion: A new derivation and its
839 implication for the modeling of bedrock channel morphology: *J. Geophys. Res.*, 112,
840 doi:10.1029/2006JF000697, 2007.

841 Turowski, J.M., Hovius, N., Meng-Long, H., Lague, D., and Men-Chiang, C.: Distribution of erosion
842 across bedrock channels: *Earth Surf. Process. Landforms*, 33, 353-363, doi:10.1002/esp.1559, 2008.

843 Whipple, K.X., and Tucker, G.E.: Dynamics of the stream-power river incision model: Im- plications
844 for height limits of mountain ranges, landscape response timescales, and research needs: *Journal of*
845 *Geophysical Research*, v. 104, p. 17,661–17,674, 1999.

846 Whittaker, A.C., and Boulton, S.J.: Tectonic and climatic controls on knickpoint retreat rates and
847 landscape response times: *Journal of Geophysical Research*, v. 117, F02024, doi:10
848 .1029/2011JF002157, 2012.

849 Whittaker, A.C., Cowie, P.A., Attal, M., Tucker, G.E., and Roberts, G.P.: Bedrock channel adjustment
850 to tectonic forcing: Implications for predicting river incision rates: *Geology*, v. 35, p. 103,
851 doi:10.1130/G23106A.1, 2007.

852 Wickert, A.D., Martin, J.M., Tal, M., Kim, W., Sheets, B., and Paola, C.: River channel lateral
853 mobility: Metrics, time scales, and controls: *J. Geophys. Res.-Earth*, 118, 396-412,
854 doi:10.1029/2012JF002386, 2013.

855 Zavala-Ortiz, V., Carretier, S., Regard, V., Bonnet, S., Riquelme, R., and Choy, S.: Along-stream
856 variations in valley flank erosion rates measured using ^{10}Be concentrations in colluvial deposits from
857 canyons in the Atacama Desert: *Geophysical Research Letters*, 48, doi:10.1029/2020GL089961, 2021.